Sarcolemmal ATP-sensitive potassium channels modulate skeletal muscle function under low-intensity workloads

Zhiyong Zhu,[1] Ana Sierra,[1] Colin M.-L. Burnett,[1] Biyi Chen,[1] Ekaterina Subbotina,[1] Siva Rama Krishna Koganti,[1] Zhan Gao,[1] Yuejin Wu,[1] Mark E. Anderson,[1,2] Long-Sheng Song,[1,2] David J. Goldhamer,[3,4] William A. Coetzee,[5] Denice M. Hodgson-Zingman,[1,2] and Leonid V. Zingman[1,2,6]

[1]Department of Internal Medicine and [2]Fraternal Order of Eagles Diabetes Research Center, University of Iowa Carver College of Medicine, Iowa City, IA 52242
[3]Center for Regenerative Biology and [4]Department of Molecular and Cell Biology, Advanced Technology Laboratory, University of Connecticut, Storrs, CT 06269
[5]Department of Pediatrics, New York University School of Medicine, New York, NY 10016
[6]Department of Veterans Affairs Medical Center, Iowa City, IA 52242

ATP-sensitive potassium (K_{ATP}) channels have the unique ability to adjust membrane excitability and functions in accordance with the metabolic status of the cell. Skeletal muscles are primary sites of activity-related energy consumption and have K_{ATP} channels expressed in very high density. Previously, we demonstrated that transgenic mice with skeletal muscle–specific disruption of K_{ATP} channel function consume more energy than wild-type littermates. However, how K_{ATP} channel activation modulates skeletal muscle resting and action potentials under physiological conditions, particularly low-intensity workloads, and how this can be translated to muscle energy expenditure are yet to be determined. Here, we developed a technique that allows evaluation of skeletal muscle excitability in situ, with minimal disruption of the physiological environment. Isometric twitching of the tibialis anterior muscle at 1 Hz was used as a model of low-intensity physical activity in mice with normal and genetically disrupted K_{ATP} channel function. This workload was sufficient to induce K_{ATP} channel opening, resulting in membrane hyperpolarization as well as reduction in action potential overshoot and duration. Loss of K_{ATP} channel function resulted in increased calcium release and aggravated activity-induced heat production. Thus, this study identifies low-intensity workload as a trigger for opening skeletal muscle K_{ATP} channels and establishes that this coupling is important for regulation of myocyte function and thermogenesis. These mechanisms may provide a foundation for novel strategies to combat metabolic derangements when energy conservation or dissipation is required.

The Journal of General Physiology

INTRODUCTION

ATP-sensitive potassium (K_{ATP}) channels have the unique ability to adjust membrane electrical properties and functions in accordance with the metabolic status of the cell (Noma, 1983; Ashcroft, 1988; Lederer and Nichols, 1989; Weiss and Venkatesh, 1993; Vivaudou and Forestier, 1995; Aguilar-Bryan and Bryan, 1999; Flagg et al., 2010; MacIntosh et al., 2012). K_{ATP} channels are widely expressed in various excitable tissues including brain, pancreas, smooth muscle, heart, and skeletal muscle (Zingman et al., 2003; Minami et al., 2004; Flagg et al., 2010; Kefaloyianni et al., 2012; MacIntosh et al., 2012). Different isoform combinations of the channel subunits contribute to tissue-specific properties (Ashcroft, 1988; Aguilar-Bryan and Bryan, 1999; Flagg et al., 2010). Skeletal muscle K_{ATP} channels are predominantly formed through physical association of four pore-forming potassium channel subunits, Kir6.2, a weak inward rectifier, with four regulatory sulfonylurea receptor subunits, SUR2A, and significantly less expression of SUR1 and Kir6.1 subunits (Flagg et al., 2010). Metabolic sensing by the channel occurs through modulation of the K^+ pore ATP sensitivity by the SUR subunit, which is also required for channel activation by MgADP and potassium channel openers as well as inhibition by sulfonylurea drugs (Noma, 1983; Ashcroft, 1988; Lederer and Nichols, 1989; Nichols and Lederer, 1991; Inagaki et al., 1995; Shyng et al., 1997; Aguilar-Bryan and Bryan, 1999; Schwappach et al., 2000; Zingman et al., 2001, 2007; Seino and Miki, 2003; Flagg et al., 2010).

Cardiac and skeletal muscles are primary sites of physical activity–related energy consumption and have K_{ATP} channels expressed in very high density (Noma, 1983; Nichols and Lederer, 1991; Seino and Miki, 2003; Thabet et al., 2005; Alekseev et al., 2010; Flagg et al., 2010; Kristensen and Juel, 2010). In the heart, K_{ATP} channel opening occurs

Correspondence to Leonid V. Zingman: leonid-zingman@uiowa.edu

Abbreviations used in this paper: APD, action potential duration; FDB, flexor digitorum brevis; K_{ATP}, ATP-sensitive potassium; KO, Kir6.2 knockout; TA, tibialis anterior; TG, transgenic.

The Rockefeller University Press $30.00
J. Gen. Physiol. Vol. 143 No. 1 119–134
www.jgp.org/cgi/doi/10.1085/jgp.201311063

in response to numerous stressors associated with either reduced energy availability, such as hypoxia or ischemia (Suzuki et al., 2002; Zingman et al., 2002; Zhu et al., 2011; Nichols et al., 2013), or increased energy utilization, including heart rate acceleration within the normal, physiological range (Alekseev et al., 2010; Zingman et al., 2011; Sierra et al., 2013). The resultant cellular potassium efflux promotes action potential shortening, thus limiting the drive for calcium influx and calcium-induced calcium release (Zingman et al., 2002). This conserves cellular energy that would otherwise be used for calcium homeostasis and contraction (Alekseev et al., 2010; Zingman et al., 2011). A shortened action potential duration (APD) also results in a longer diastolic interval, critical for energy resource replenishment (Alekseev et al., 2010; Zingman et al., 2011). Thus, a central role of ventricular myocyte K_{ATP} channels is fine-tuning of the APD to optimize cardiac function across a wide range of workloads while avoiding depletion of cellular metabolic resources that could lead to injury or dysfunction (Zingman et al., 2002, 2003, 2011; Zhu et al., 2011).

Understanding of the physiological role of K_{ATP} channels in skeletal muscle has lagged behind that of its cardiac analogues. So far skeletal muscle K_{ATP} channel opening has been linked to prevention of calcium overload and preservation of myofiber integrity during high-intensity endurance exercise as well as recovery from fatiguing programs of contraction (Light et al., 1994; Matar et al., 2000, 2001; Renaud, 2002; Gong et al., 2003; Thabet et al., 2005; Cifelli et al., 2007, 2008; Flagg et al., 2010; MacIntosh et al., 2012). In addition, we previously demonstrated that transgenic mice with skeletal muscle–specific disruption of K_{ATP} channel function consume more energy than WT littermates because of reduced muscle energy efficiency, even during very low-intensity physical activity (Alekseev et al., 2010). However, it is not yet fully understood how K_{ATP} channel activation modulates skeletal muscle resting and action potentials under physiological conditions, particularly low-intensity workloads, and how this can be translated to muscle energy usage.

Here, we used a novel technique to evaluate skeletal myofiber excitability in situ to demonstrate that skeletal muscle K_{ATP} channel opening can be triggered by non-fatiguing workloads. The consequent changes in resting and action potentials were coupled with moderated dynamics of calcium release, force, and heat generation. Thus, this study defines an energy-sparing function of skeletal muscle K_{ATP} channels under low-intensity workloads.

MATERIALS AND METHODS

Mouse models

All animal protocols conform to the Guide for the Care and Use of Laboratory Animals generated by the Institute for Laboratory Animal Research, National Research Council of the National Academies, and were approved by the University of Iowa Institutional Animal Care and Use Committee.

98 male mice aged 10–12 wk were used for all experiments. The strains used were Kir6.2 knockout (KO) mice (Miki et al., 1998; Zingman et al., 2002; Alekseev et al., 2010), which have whole-body deletion of the Kir6.2 isoform of the K_{ATP} channel pore-forming subunit, and their C57BL/6 WT controls and Kir6.1-AAA Tg (Tong et al., 2006) crossed with MyoD-Cre Tg (Chen et al., 2005; TG) mice (Alekseev et al., 2010), which have skeletal muscle–specific transgenic interference with normal sarcolemmal K_{ATP} channel function through expression of a nonfunctional, dominant-negative inhibitory, pore-forming subunit and their WT FVB controls. For harvesting of tissue samples and for all other nonsurvival experiments, mice were anesthetized (Avertin: 2.5% solution of tribromoethanol in 2-methyl-2-butanol; Sigma-Aldrich; 240 mg/kg i.p.) and supplied with continuous inhaled isoflurane (~1.0–1.5%; Piramal Healthcare) via a nose cone to maintain a respiratory rate of ~50–60 breaths per minute. At the end of experiments, mice were euthanized by cardiectomy while under anesthesia with inhaled isoflurane.

Solutions

Tyrode's solution in mmol/liter was as follows: 136.5 NaCl, 5.4 KCl, 2.5 $CaCl_2$, 0.53 $MgCl_2$, 5.5 glucose, and 5.5 HEPES-NaOH, pH 7.4. Internal pipette solution in mmol/liter was as follows: 140 KCl, 1 $CaCl_2$, 1 $MgCl_2$, and 5 HEPES-KOH, pH 7.4.

Experimental apparatus

Anesthetized mice were placed on a platform (809B; Aurora Scientific) heated by circulating water (6200 R20F; Thermo Fisher Scientific). The tibialis anterior (TA) muscle of one leg was exposed and the tendons attached to the force transducer (305C; Aurora Scientific). Tyrode's solution warmed to 30.0°C was dripped on the muscle at ~1 drop/s. The temperature of the platform on which the mouse was placed was maintained by circulating heated water at 34.8°C. These two methods stabilized the temperature measured at the surface of the muscle at ~30°C. A stimulator (Accupulser A310; World Precision Instruments) routed through a stimulus isolation unit (A365 SIU; World Precision Instruments) was used to excite the sciatic nerve (variable amplitude, pulse width 0.5 ms using a custom electrode). Pacing triggers were generated and data collected at 25 kHz using pCLAMP software (Molecular Devices) interfaced with a digital acquisition device (Digidata 1440A; Molecular Devices). The experimental apparatus, including force transduction platform, force transducer, microelectrode head stage (see below), and micromanipulators, was located on a vibration isolation table (VH3648; Newport) inside a Faraday cage (FC3648; Newport).

Microelectrode recordings

Pipettes were pulled on a horizontal puller (P-1000; Sutter Instrument) using borosilicate glass (1B150F; World Precision Instruments). The tip of each pipette was filled with 3 M KCl. A 0.005-in diameter silver wire coated with polytetrafluoroethylene (PTFE) was mechanically stripped at both ends and electrochemically plated with silver chloride on one end to produce an Ag/AgCl electrode. The wire was coiled around a cylinder (~1-cm diameter) by one turn to produce a helical spring-like shape in the middle. The micropipette was scored with a carbide utility blade ~1–2 mm above the shoulder and the shank gently separated from the tip. The silver chloride–coated end of the wire was inserted into the glass tip sufficiently to create enough friction to support the weight of the tip (Zhou et al., 1992). The opposite end of the silver wire was attached to the amplifier head stage (CV203-BU; Molecular Devices). A silver chloride–coated reference wire was placed in contact with the lateral edge of the exposed muscle using a salt bridge. The tip resistance of the microelectrode was measured

(7–20 MΩ), and zero potential was adjusted before each impalement with the floating microelectrode and reference in a bath of Tyrode's solution. Each impalement was performed with a new microelectrode. Action potentials were amplified (Axopatch 200B; Molecular Devices) and recorded at 25 kHz using pCLAMP software (Molecular Devices) interfaced with a digital acquisition device (Digidata 1440A; Molecular Devices).

Action potentials were analyzed if all of the following criteria were met: (a) the measured potential showed a sharp drop upon microelectrode penetration, (b) the resting membrane potential was more negative than −70 mV, (c) the overshoot was >0 mV, and (d) the stimulus artifact did not interfere with the upstroke of the action potential. The resting membrane potential was measured from the baseline before the action potential. Overshoot was defined as the difference in potential between the peak of the action potential and 0 mV. Action potential amplitude was defined as the difference between resting membrane potential and the peak potential. APD was defined as the duration at −40 mV.

Force measurements

The force transducer/controller (305C; Aurora Scientific, Fig. 1) was set for isometric contraction. Muscle twitches were provoked by sciatic nerve stimulation. The resting tension on the muscle was set by incrementally adjusting the controller lever arm, and thus muscle length (L_0) and resting tension, and then delivering a supramaximal stimulus to the sciatic nerve until a maximal twitch force was obtained. The resting tension at L_0 was then recorded, typically ∼75 mN. The stimulation amplitude was then set by plotting a twitch force versus stimulus amplitude curve and then setting the stimulator output at two times the threshold for a maximal twitch. Twitch force was normalized to the calculated muscle cross-sectional area (mN/cm^2) using the muscle mass (in g) divided by the product of the presumed muscle density of 1.06 g/cm^3 and the optimal fiber length ($L_0 \times 0.6$, in cm) and expressed as specific force (Brooks and Faulkner, 1988; Hakim et al., 2011). L_0 was measured between suture knots on the muscle tendon and muscle mass was measured in muscles excised at the suture knots.

Body surface temperature

The body surface temperature of the mice was imaged using a high-resolution infrared camera (A655sc Thermal Imager; FLIR Systems, Inc.). Quantitative analysis of infrared images was performed using FLIR ResearchIR software version 3.4.13039.1003. Mice were imaged on a multilane treadmill next to their age-matched littermate controls at baseline and after 6 min of treadmill exercise at 7 m/min and 15° incline (Zingman et al., 2002). Images were obtained every 1 s. The side by side imaging of mice in the same camera frame allows simultaneous assessment and direct comparison of the body surface heating in the different mouse models providing an advantage over other methods for assessing body temperature that would be limited by the accuracy and concordance of two separate temperature probes.

TA temperature

Anesthetized mice were placed on the on the experimental apparatus (see above). The TA tendons of one leg were exposed and attached to the force transducer (305C; Aurora Scientific). A flexible implantable thermocouple microprobe IT-23 (Physitemp Instruments, Inc.) was inserted under the muscle fascia adjacent to the tibia without disruption of muscle integrity. The skin was closed with 6.0 Ethilon suture to prevent heat loss. The TA muscle was subjected to repetitive isometric contractions via sciatic nerve stimulation as described above. Differential thermal analysis of TA muscle (heated platform with constant temperature was used as a reference) was conducted using a BAT-10 Multipurpose Thermometer (Physitemp Instruments, Inc.) that allows measuring of differential temperature in the physiological range with 0.01°C accuracy.

Histology

TA muscles were dissected from anesthetized mice. Muscles were embedded in OCT compound and frozen in 2-methylbutane precooled at −165°C in liquid nitrogen. Muscles were stored at 80°C until used. For histology, 10-µm cross sections, cut using a Microm cryostat, cooled to −23°C, were mounted on positively charged slides (Superfrost/Plus; Thermo Fisher Scientific) and stored at −80°C until used. Immunohistochemical analysis was used to determine the fiber type composition of the muscles. Serial cross sections of TA were double-labeled with anti-laminin primary antibody and either anti–MHC I, IIA, IIB, or IIX antibodies (A4.951 anti–MHC I mouse IgG, SC-71 anti–MHC IIA mouse IgG, 6H1 anti–MHC IIX mouse IgM, and FB-F3 anti–MHC IIB mouse IgM [Developmental Studies Hybridoma Bank] and anti-laminin

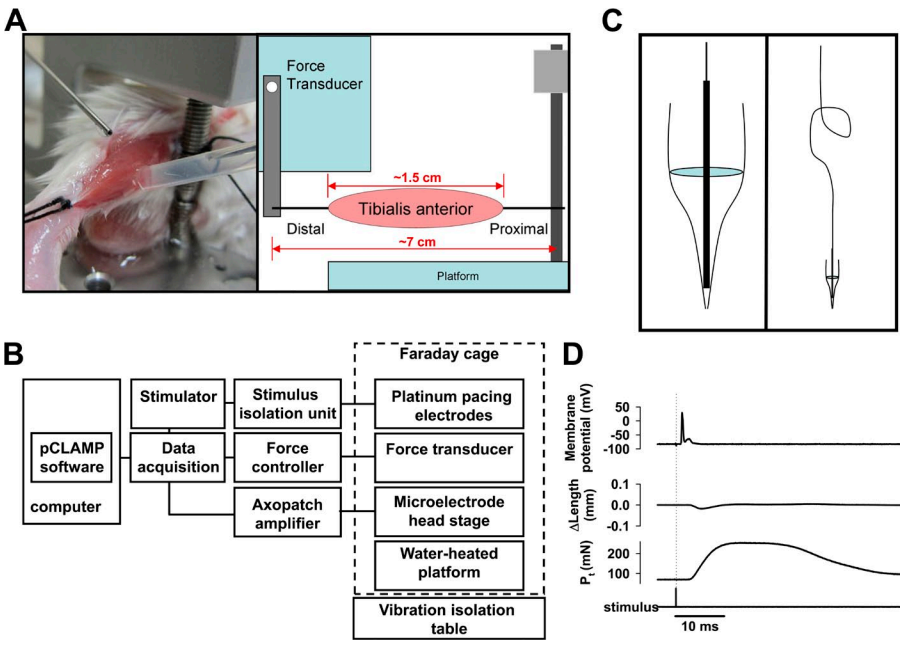

Figure 1. Experimental apparatus for in situ skeletal muscle force and action potential measurement. (A) The anesthetized mouse lying on a warmed platform has the exposed TA muscle attached proximally to a fixed pillar and distally to the lever arm of the force feedback controller. Tyrode's solution is dripped on the muscle to prevent drying. A reference electrode is in contact with the muscle via a salt bridge. (B) The apparatus is organized as illustrated. (C) The floating intracellular microelectrode is created by wedging the silver chloride–coated tip of a fine silver wire into the tip of a glass microelectrode filled with 3 M KCl (left). An ∼1-cm-diameter helical curve is formed in the midsection of the silver wire to buffer small movements of the muscle (right). (D) A representative recording obtained during isometric contraction of the TA in response to a single sciatic nerve stimulus: action potential (top), change in muscle length (middle), and muscle force (Pt; bottom).

rabbit IgG [Sigma-Aldrich]). Slides were then incubated with secondary antibodies (Alexa Fluor 568 anti–rabbit and Alexa Fluor 488 anti–mouse anti-IgG and IgM as appropriate; Life Technologies). For nuclei staining, the sections were incubated with TO-PRO 3. Sections were mounted with Vectashield reagent and stored at −80°C until imaged. Control sections were also stained without the primary antibody to test for nonspecific secondary antibody binding.

Single cell calcium imaging

Flexor digitorum brevis (FDB) muscles were used because of their small size, ease of isolation, high K_{ATP} channel expression, and similar fiber type composition to TA muscles (Banas et al., 2011). Skeletal muscle fibers were enzymatically isolated (Alekseev et al., 2010; Lueck et al., 2010) and loaded with 5 µM Rhod-2 AM (40 min) at room temperature. After de-esterification, the cells were placed in a recording chamber and perfused with normal Tyrode's solution (1.8 mM Ca^{2+}) at 37°C. Confocal Ca^{2+} imaging was performed with a laser-scanning confocal microscope (LSM 510 Meta; Carl Zeiss) equipped with an NA 1.35, 63× lens. Line scan measurements of Ca^{2+} transients were acquired at a sampling rate of 1.93 ms/line along the longitudinal axis of the fibers. Steady-state Ca^{2+} transients were achieved by continuous 1-Hz field stimulation. All digital images were processed with IDL 6.0 software (Research System Inc.; Song et al., 2006).

To quantitatively assess resting cytosolic Ca^{2+} concentration, myocytes were incubated with 5 µM Fura-2 AM (Molecular Probes) for 25 min at room temperature and then perfused with Tyrode's solution (1.8 mM Ca^{2+}) for 25 min at 36°C to wash out the dye in the solution. Myocytes were paced at 1 Hz by an SIU-102 (Warner Instruments) controlled by Clampex 10 software. Ca^{2+} images were collected by an Eclipse microscope (Nikon) with 40× oil objectives. Fura-2 ratio was obtained by excitation at 340 and 380 nM using a DG-4 (Sutter Instrument) and emission at 510 nM at ∼113 frames/s. Imaging acquisition and processing was controlled by Nikon NIS Elements AR software. All data were collected 30 ± 0.5°C.

Single channel recordings

As with Ca^{2+} imaging, FDB muscles were used to obtain isolated myofibers. Single muscle fibers were enzymatically isolated (Alekseev et al., 2010; Lueck et al., 2010), and single channel currents were recorded in the cell-attached mode using an Axopatch 200B amplifier (Molecular Devices) integrated with a TE2000-U microscope (Nikon). A command potential of −10 mV was set in a pipette filled with internal pipette solution, resistance of 5–7 MΩ. Cells were bathed in Tyrode's solution (1.8 mM Ca^{2+}). Experiments were performed at 30°C using a temperature controller TC2r (Cell MicroControls). K_{ATP} channel opening was induced by 5 min of 1-Hz field stimulation. Membrane seals were formed within 20–40 s after cessation of stimulation. Data were recorded at 25 kHz using pCLAMP software (Molecular Devices) interfaced with a digital acquisition device (Digidata 1440A; Molecular Devices). A longer stimulation time at 1 Hz was used here (5 min) to account for the 20–40-s delay in forming a patch during which time the cell is expected to begin metabolic recovery toward resting state with consequent reduction in K_{ATP} channel opening, in contrast to calcium imaging (1 min) where measurements were taken during the applied workload.

Statistics

Results are expressed as mean ± SEM. Comparisons between two groups were made using the two-sided Student's *t* test and between more than two groups using ANOVA as indicated in the figure legends. A p-value < 0.05 was considered statistically significant. Sigma Plot 11 was used for all statistical analyses.

RESULTS

Approach for evaluation of muscle transmembrane potentials in situ

The muscle natural environment may significantly affect skeletal muscle fiber electrophysiological properties (Matar et al., 2001; MacIntosh et al., 2012). However, measurement of single muscle fiber membrane excitability within a largely preserved mechanical and chemical environment has remained elusive because of limitations on recordings imposed by motion. When in situ transmembrane recordings have been made, they could only be performed in muscles that were not actively contracting (Skirboll et al., 1979; Hicks and McComas, 1989). To address this problem, we developed a novel approach for measuring single skeletal muscle fiber transmembrane potentials in situ using a floating microelectrode (Zhou et al., 1992).

In anesthetized mice, the TA muscle of one leg was exposed through dissection of the skin and removal of the muscle fascia. A 3-0 silk suture was tied around the patellar tendon and secured to the fixed pillar of the force transducer. A 3-0 silk suture was tied around the distal tendon and looped through the lever arm of the force transducer. The TA was continuously superfused with Tyrode's solution (Fig. 1 A). The experimental apparatus, including heated force transduction platform, force transducer, microelectrode head stage, and micromanipulators, was situated on a vibration isolation table inside a Faraday cage to minimize artifact (Fig. 1 B).

Floating microelectrodes were made using traditional borosilicate intracellular glass pipettes filled with 3 M KCl. The micropipette was scored with a carbide utility blade and the shank gently separated from the tip. The tip was then placed on the silver chloride–coated end of a 0.005-in-diameter silver wire shaped with an ∼1-cm-diameter helical spring in the center (Fig. 1 C). A silver chloride–coated reference wire was placed in contact with the lateral edge of the exposed muscle using a salt bridge (Fig. 1 A). A single isometric twitch with resulting action potential, change in muscle length, and generated force are shown (Fig. 1 D). Thus, this approach would allow for the measurement of single fiber transmembrane potentials in a minimally disrupted in situ environment.

Effects of pharmacologic K_{ATP} channel activation on skeletal muscle transmembrane potentials in situ

Isolated muscle and fiber studies have been essential in demonstrating the importance of K_{ATP} channel activity on muscle fiber electrical properties (Light et al., 1994; Matar et al., 2000; Gong et al., 2003; Thabet et al., 2005; Cifelli et al., 2007, 2008; Flagg et al., 2010; Kristensen and Juel, 2010; MacIntosh et al., 2012). However, it remains unknown whether the changes seen reflect K_{ATP} channel function in situ.

We chose to study the TA muscle because of its predominantly fast, glycolytic fibers, which have been linked to high expression of K_{ATP} channels (Kristensen and Juel, 2010; Banas et al., 2011), and its easy accessibility for our microelectrode and force measurements (Brooks and Faulkner, 1988; Hakim et al., 2011). In WT mice, we examined sequential cross sections of TA to determine fiber type and distribution. We confirmed that the TA (Fig. 2 A) is composed of type IIB and type IIX fibers (Fig. 2, C and D) with little or no contribution by type IIA or type I fibers (Fig. 2, E and F) and that this distribution was unchanged in models with genetic deletion (KO) or dominant-negative inhibition (TG) of sarcolemmal K_{ATP} channels (Fig. 2 G; Zhang et al., 2010). We probed adjacent sections of WT TA for Kir6.2 and found its presence to a variable degree in all fibers (Fig. 2 B), although greater overall in IIX versus IIB fibers (Fig. 2 H).

To evaluate the effect of K_{ATP} channel opening on resting and action potentials in situ, we superfused the exposed TA muscle for at least 20 min with either Tyrode's solution containing 100 µM of the potassium channel opener Pinacidil (Sigma-Aldrich), a potent activator of skeletal muscle K_{ATP} channels (Ashcroft and Gribble, 2000; Matar et al., 2000; Moreau et al., 2000; Gong et al., 2003; Alekseev et al., 2010), or the combination of 100 µM Pinacidil and 10 µM of the specific K_{ATP} channel blocker glyburide (Sigma-Aldrich; Zingman et al., 2011). To assay TA membrane excitability under resting conditions, the sciatic nerve was paced using a single stimulus (approximately one repetition per minute). Measurements of the resting membrane potential and action potential were compared before and after the pharmacologic activation ± blockade of K_{ATP} channels (Fig. 3). We found that exposure to Pinacidil resulted in a significant hyperpolarization of the resting potential, with reduction in action potential overshoot and APD at −40 mV (APD_{-40mV}; Fig. 3). These changes were significantly diminished in the presence of glyburide (Fig. 3). In agreement with the literature (Gramolini and Renaud, 1997), our preliminary experiments did not reveal any effect of glyburide alone on action potentials (not depicted), and so this condition was not further studied.

To further confirm dependence of the observed Pinacidil-induced changes of resting and action potential on K_{ATP} channel function, the same experiments were performed in two genetic mouse models. The first model (KO) has global disruption of the gene for the Kir6.2 subunit of K_{ATP} channels (Zingman et al., 2002; Gong et al., 2003; Seino and Miki, 2003; Alekseev et al., 2010). We found that at baseline, KO mice had a similar resting potential, overshoot and APD_{-40mV} compared with their WT controls (Fig. 3, A–D). In response to Pinacidil, these parameters were unchanged in the KO mice (Fig. 3, A–D). In a second model (TG), K_{ATP} channel function was selectively disrupted in skeletal muscle through expression of a dominant-negative, nonconducting potassium pore mutant (Malester et al., 2007) under control of the Myo-D promoter (Chen et al., 2005; Alekseev et al., 2010). We found that at rest, TA in these TG mice had a similar resting potential, overshoot, and APD_{-40mV}

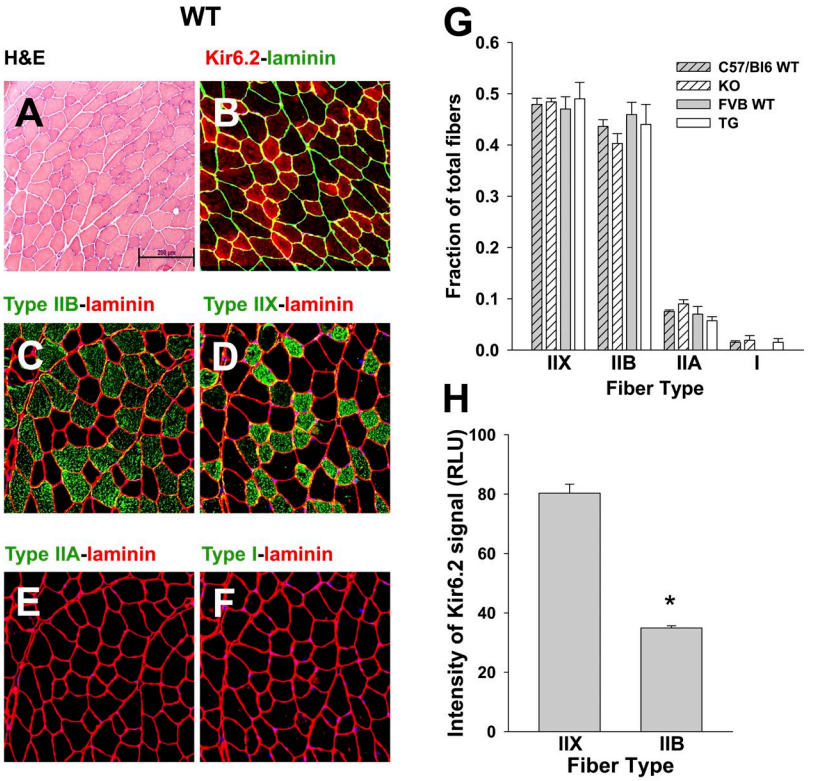

Figure 2. Murine TA is composed of predominantly IIB and IIX fiber types with variable K_{ATP} channel expression. Sequential transverse sections of FVB WT mouse TA muscle are displayed to illustrate the distribution of muscle fiber types and Kir6.2 expression. (A) Hematoxylin and eosin (H&E). (B) Immunolabeling of Kir6.2 and laminin. (C–F) Immunolabeling of fiber type and laminin. Bar, 200 µm. (G) The composition of fibers for C57BL/6 WT TA is 47.9 ± 1.2% type IIX, 43.6 ± 1.3% type IIB, 7.5 ± 0.3% type IIA, and 1.5 ± 0.3% type I (n = 3 mice, 10,749 fibers), for KO is 48.4 ± 0.7% type IIX, 40.3 ± 1.9% type IIB, 9.0 ± 0.8% type IIA, and 1.9 ± 0.9% type I (n = 3 mice, 10,262 fibers), for FVB WT is 47.0 ± 2.4% type IIX, 45.9 ± 2.4% type IIB, 7.0 ± 1.5% type IIA, and no observations of type I (n = 3 mice, 10,694 fibers), and for TG is 49.0 ± 3.2% type IIX, 44 ± 3.9% type IIB, 5.7 ± 0.8% type IIA, and 1.5 ± 0.7% type I (n = 3 mice, 10,221 fibers). There are no significant differences in percentage of fiber type between mouse groups by ANOVA. (H) The intensity of Kir6.2 immunofluorescence in FVB WT type IIX fibers (80.33 ± 3.03 relative light units [RLU], n = 26 fibers) is more than double that in IIB fibers (34.90 ± 0.74 RLU, n = 43 fibers; *, $P < 0.05$ by Mann–Whitney rank sum test). Error bars indicate SEM.

compared with that of WT controls (Fig. 3, E–H). In response to Pinacidil, the changes in resting potential and APD_{-40mV} seen with WT were absent in TG mice (Fig. 3, E–H). There was a similar overshoot reduction in both WT and TG mice; however, in TG mice the reduction was glyburide insensitive in contrast to the overshoot reduction in WT, which was entirely abolished by glyburide (Fig. 3 G). We interpret the Pinacidil-dependent, glyburide-insensitive effect on action potential overshoot in the TG as the result of the nonspecific influence of Pinacidil on other channels that may be up-regulated in TG in response to the genetic modification, making these effects detectable in TG but not in WT mice.

In light of the variable level of Kir6.2 expression and the presence of two populations of myofiber types (IIB and IIX) in the TA muscle (Fig. 2), we also examined the distribution of the observed resting potential and action potential parameters in response to Pinacidil. A continuum of values, rather than segregation into distinct groups (Fig. 4), indicates that even a relatively reduced expression of Kir6.2 in IIB muscle fibers compared with IIX is sufficient to elicit comparable responses in the resting and action potentials under our experimental conditions. Thus, our data indicate that pharmacologic skeletal muscle K_{ATP} channel opening in situ causes significant membrane hyperpolarization, reduced action potential overshoot, and shortened APD.

K_{ATP} channels regulate skeletal muscle transmembrane potentials in response to low-intensity workloads

Previous electrophysiological evaluation of K_{ATP} channel effects on muscle fiber membrane electrical properties has been performed in the setting of extreme, fatiguing workloads or through the use of pharmacologic openers or inhibitors (Light et al., 1994; Gong et al., 2003; Thabet et al., 2005; Cifelli et al., 2007; Flagg et al., 2010; MacIntosh et al., 2012). However, even at low-intensity workloads, skeletal muscle K_{ATP} channel function has been linked to improved whole-body energy efficiency (Alekseev et al., 2010). Specifically, mice with knockout of the Kir6.2 subunit or with skeletal muscle–specific transgenic reduction in functioning K_{ATP} channels, the same models used here, display increased energy expenditure and reduced body weight under nonexercise activity compared

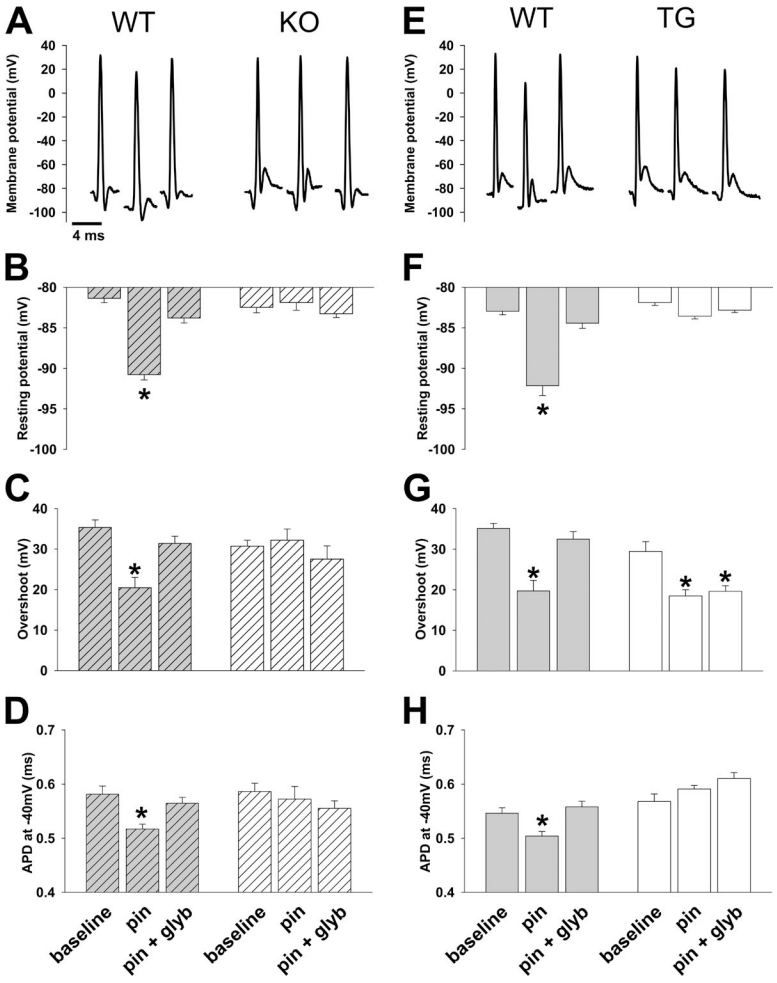

Figure 3. Pharmacologic activation of K_{ATP} channels results in significant changes in skeletal muscle action potential morphology. Representative action potentials and summary statistics for action potential morphology in TA muscle in situ are shown for TG and KO with their respective WT controls under the conditions indicated along the bottom of the figure: baseline, pin (Pinacidil exposure), and pin + glyb (Pinacidil + glyburide exposure). Summary statistics for WT (gray with stripes) and KO (open with stripes) are shown on the left (n = 32, 27, and 42 and 48, 13, and 12 APs from n = 5, 6, and 4 and 6, 3, and 3 mice, respectively; *, $P < 0.05$ vs. baseline using Student's t test and Mann–Whitney rank sum test) and for WT (gray) and TG (open) shown on the right (n = 57, 22, and 37 and 20, 55, and 55 APs from n = 10, 5, and 3 and 6, 7, and 7 mice, respectively; *, $P < 0.05$ vs. baseline using Student's t test and Mann–Whitney rank sum test) under their respective representative action potential. (A–D) Shown for WT controls with KO are representative action potentials (A), resting potential (−81.4 ± 0.5 mV, −90.8 ± 0.7 mV, and −83.8 ± 0.6 mV for WT and −82.5 ± 0.7 mV, −81.9 ± 1 mV, and −83.3 ± 0.5 mV for KO; B), action potential overshoot (35.3 ± 1.9 mV, 20.5 ± 2.5 mV, and 31.4 ± 1.8 mV for WT and 30.7 ± 1.5 mV, 32.2 ± 2.8 mV, and 27.5 ± 3.2 mV for KO; C), and APD_{-40mV} (0.58 ± 0.02 ms, 0.52 ± 0.01 ms, and 0.57 ± 0.01 ms for WT and 0.59 ± 0.02 ms, 0.57 ± 0.02 ms, and 0.56 ± 0.01 ms for KO; D). (E–H) Shown for WT controls with TG are representative action potentials (E), resting potential (−83.0 ± 0.4 mV, −92.1 ± 1.2 mV, and −84.4 ± 0.6 mV for WT and −81.9 ± 0.4 mV, −83.6 ± 0.3 mV, and −82.8 ± 0.3 mV for TG; F), action potential overshoot (35.1 ± 1.3 mV, 19.7 ± 2.6 mV, and 32.5 ± 1.8 mV for WT and 29.4 ± 2.5 mV, 18.5 ± 1.5 mV, and 19.6 ± 1.4 mV for TG; G), and APD_{-40mV} (0.55 ± 0.01 ms, 0.50 ± 0.01 ms, and 0.56 ± 0.01 ms for WT and 0.57 ± 0.01 ms, 0.59 ± 0.01 ms, and 0.61 ± 0.01 ms for KO; H). Error bars indicate SEM.

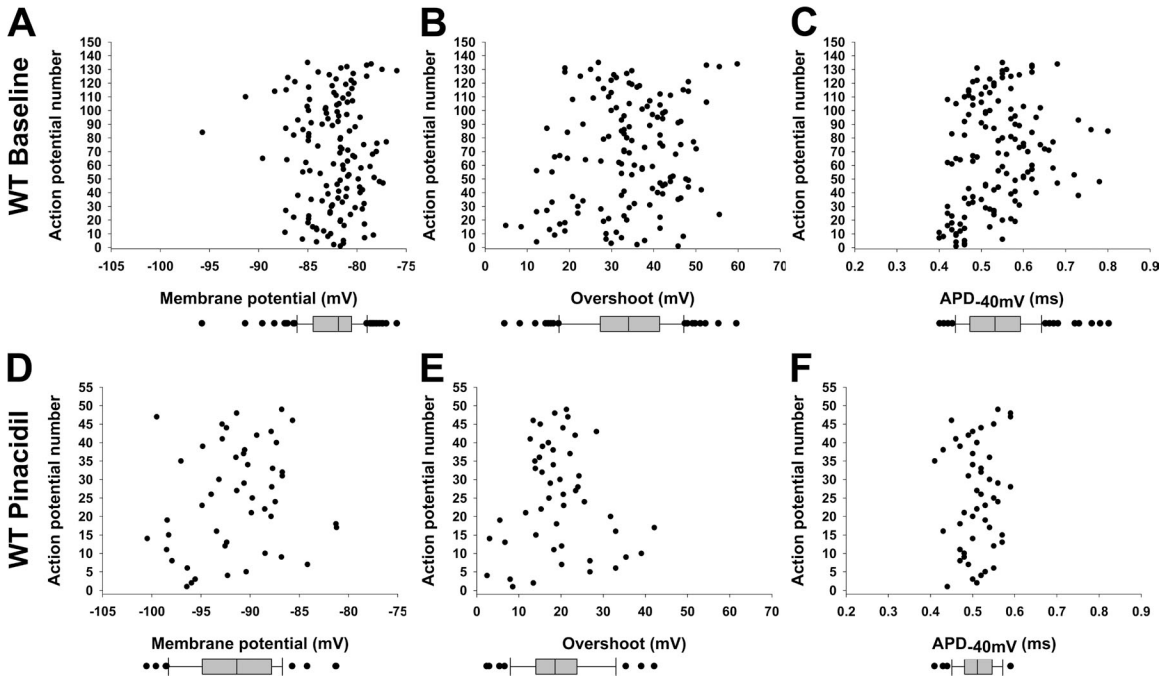

Figure 4. Resting and action potential parameter populations with and without K_{ATP} channel activation. The resting potential and action potential parameters from in situ TA muscle of WT mice are plotted against action potential number to illustrate their distribution. Baseline data for Pinacidil experiments (Fig. 3) and twitching experiments (Fig. 7) and data for FVB (controls for TG) and C57BL/6 WT (controls for KO) are combined for this graphic to increase numbers. Box and whisker plots are shown below each distribution, indicating median, upper and lower quartile, and outliers (>1.5 times upper and lower quartiles). (A–C) Shown for baseline conditions ($n = 135$) are resting potential (median −82.9 mV; A), overshoot (median 34.2 mV; B), and APD_{-40mV} (median 0.53 ms; C). (D–F) Shown for Pinacidil effect ($n = 49$) are resting potential (median −91.4 mV; D), overshoot (median 18.5 mV; E), and APD_{-40mV} (median 0.51 ms; F).

with their WT controls (Alekseev et al., 2010). Here, we examined how K_{ATP} channel function affects in situ skeletal muscle transmembrane resting and action potentials in response to low-intensity workloads. To assess transmembrane electrical properties under resting conditions, we twitched the muscle no more than once per minute. At this baseline, there was no significant difference in the resting tension or peak twitch force between either TG or KO and their WT controls (Tables 1 and 2). To simulate low-intensity activity (or nonexercise activity thermogenesis [NEAT]; Levine et al., 2005), we then performed 7 min of muscle twitching at 1 Hz at peak twitch force (Fig. 5). We recorded force continuously and recorded transmembrane potentials between minutes 5 and 7 of this protocol. This rate and duration of repetitive muscle twitching resulted in a small reduction in resting tension that was not significantly different between TG, KO, and their WT controls at 7 min (Table 1), whereas the dynamic of changes in specific peak force were different between muscles with intact or disrupted K_{ATP} channel function. In particular, although peak force was on average reduced between 2 and 6% in WT controls at 7 min compared with their own baselines, TG peak force remained stable and KO peak force increased on average ∼4% (Table 2).

Our simultaneous electrophysiology experiments of WT TA demonstrated significantly hyperpolarized myofiber resting potential, with reduced overshoot and APD_{-40mV}, when measured between 5 and 7 min of muscle twitching compared with these parameters at rest

TABLE 1

Muscle resting tension

Force	Time	C57BL/6 WT ($n = 9$)	KO ($n = 10$)	FVB WT ($n = 15$)	TG ($n = 19$)
	min				
Resting force (mN)	0	78.7 ± 1.5	74.8 ± 1.2	75.7 ± 0.6	77.8 ± 2.4
(P vs. WT control)			(P = NS)		(P = NS)
Δ versus baseline	7	−8.7 ± 1.7	−5.8 ± 3.1	−6.3 ± 0.6	−2.3 ± 1.4
(P vs. baseline)			(P = NS)		(P = NS)

Resting tension of in situ TA muscle is measured at time 0 (baseline) and at 7-min duration of the 1-Hz isometric twitching protocol. KO and TG mice are compared with their respective C57BL/6 and FVB controls. Measurements at time 7 min are expressed as the difference versus measurements at time 0 (p-values are for KO or TG vs. their WT controls using Student's *t* test).

TABLE 2

Muscle peak twitch force

Force	Time	C57BL/6 WT (n = 9)	KO (n = 10)	FVB WT (n = 15)	TG (n = 19)
	min				
Specific peak force (mN/cm^2)	0	4,323 ± 259	5,465 ± 471	4,471 ± 188	4,638 ± 120
(P vs. WT)			(P = NS)		(P = NS)
Δ vs. baseline	7	−87 ± 59	280 ± 69	−255 ± 53	9 ± 64
(P vs. WT)		(P = NS)	(P < 0.001)		(P = 0.004)

Peak twitch force of in situ TA muscle is measured at time 0 (baseline) and at 7-min duration of the 1-Hz isometric twitching protocol. KO and TG mice are compared with their respective C57BL/6 and FVB WT controls. Measurements at time 7 min are expressed as the mean of the difference between the peak force of each muscle at 7 min versus its own baseline force at time 0. TA muscle mass (in mg) is 50.2 ± 0.3, 49 ± 0.6, 49.2 ± 0.5, and 48.6 ± 0.23 for WT C57BL/6, KO, WT FVB, and TG, respectively (P = NS between KO or TG and their WT controls by Student's t test), and L_0 (in mm) is 15.50 ± 0.48, 15.90 ± 0.21, 14.71 ± 0.36, and 14.53 ± 1.0, respectively (P = NS between KO or TG and their WT controls using Student's t test).

(Fig. 6). This is a similar pattern compared with that for in situ Pinacidil-induced activation of K_{ATP} channels (Fig. 3 vs. Fig. 6). The changes in resting potential caused by twitching were absent in the presence of the K_{ATP} channel inhibitor, 10 μM glyburide, whereas the changes in overshoot and APD_{-40mV} were significantly attenuated (Fig. 6).

In mice with disrupted K_{ATP} channel function (KO and TG), we found no statistically significant changes in resting membrane potential and APD_{-40mV} (Fig. 6). However, as in the case of Pinacidil application, with repetitive twitching we observed a significant glyburide-insensitive reduction in overshoot (Fig. 6, C and G). We similarly interpret this as the effect of repetitive twitching on other channels, which may be up-regulated in the genetically modified mice. Thus, our findings indicate that activation of skeletal muscle K_{ATP} channels occurs in response to low-intensity workloads, resulting in significant membrane hyperpolarization, as well as reduction in both overshoot and APD_{-40mV}.

Disruption of K_{ATP} channel–dependent regulation of transmembrane potentials increases muscle thermogenesis

The vast majority of myocyte energy-dependent functions are controlled or regulated by membrane potentials. In particular, membrane potential–dependent Ca^{2+} release is a key determinant of myocyte contraction and energetics. To investigate the effect of K_{ATP} channel function on Ca^{2+} handling, we compared Ca^{2+} transients induced by 1-Hz field stimulation of isolated myofibers with intact or disrupted K_{ATP} channel function. This pacing protocol was sufficient to induce K_{ATP} channel opening in WT fibers, whereas no K_{ATP} channel activity was seen in KO or TG fibers (Fig. 7) or glyburide-treated WT fibers (not depicted). Over 1 min of 1-Hz pacing, WT fiber Ca^{2+} release exhibited a negative staircase pattern, which was blunted in the K_{ATP} channel–deficient fibers isolated from TG or KO mice (Fig. 8).There were no differences in the baseline characteristics of Ca^{2+} release in TG, KO, and their WT controls (Table 3). Furthermore,

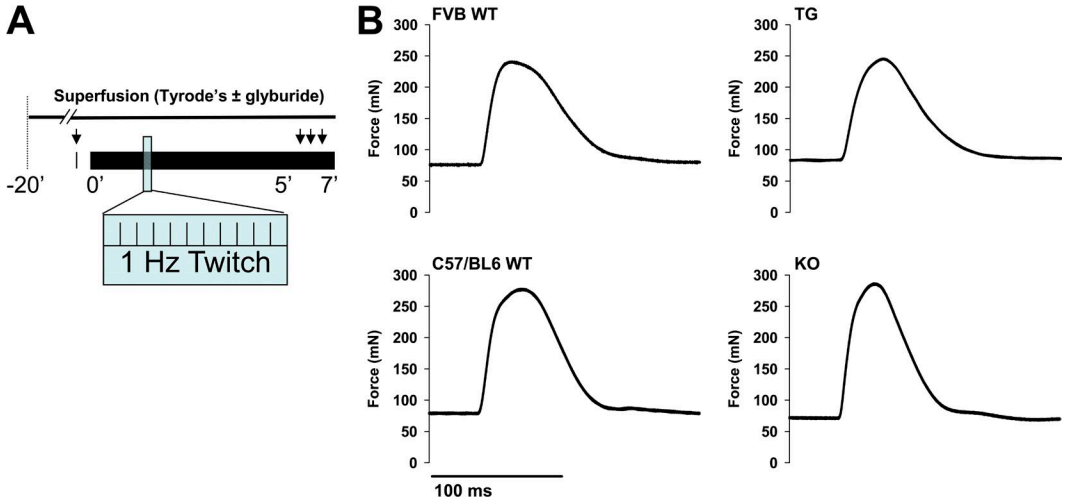

Figure 5. Isometric muscle twitch protocol simulates low-intensity exercise. (A) Schematic of the muscle twitching protocol used for in situ TA muscle. Arrows indicate time points of floating microelectrode recordings at baseline (with a single twitch to elicit an action potential) and between 5 and 7 min of repetitive twitching at 1 Hz, with and without superfusion of glyburide. (B) Representative force tracings resulting from isometric twitches of the TA muscle in TG and KO mice with their respective FVB WT and C57BL/6 WT controls.

ratiometric measurements of resting Ca^{2+} before and during exposure to pacing did not reveal significant differences between TG or KO and their corresponding WT control fibers (Table 3).

Contracting muscle uses energy for both force and heat generation. During isometric contraction, no external work is performed; thus, the muscle enthalpy is equal to the heat output (Barclay et al., 2010). Therefore, we used changes in the TA temperature under our repetitive isometric twitch protocol as an indicator of the muscle energy consumption. Specifically, we use implantable microthermocouples to measure TA temperature during our experimental protocol. There was no difference in muscle mass among groups (Table 2, legend). We found that muscles with disrupted K_{ATP} channel function in TG and KO mice exhibited significantly greater increases in their temperature compared with corresponding WT controls (Fig. 9). Furthermore, although exposed to equivalent low-intensity treadmill exercise, both KO and TG demonstrated greater body surface temperatures and greater warming over baseline than their WT controls as evaluated through measurement of the body surface temperature by infrared imaging (Fig. 10). Thus, intact K_{ATP} channel function in skeletal muscles is an important regulator of muscle calcium handling and thermogenesis.

DISCUSSION

Metabolic sensing by sarcolemmal K_{ATP} channels has historically been linked to a protective response under severe energetic insults, such as acute ischemia, sympathetic distress, endurance exercise, or intensive muscle workload associated with fatigue development (Light et al., 1994; Gong et al., 2000, 2003; Matar et al., 2000, 2001; Zingman et al., 2002; Minami et al., 2004; Thabet et al., 2005; Cifelli et al., 2007, 2008; Flagg et al., 2010; MacIntosh et al., 2012). Recently, we determined that

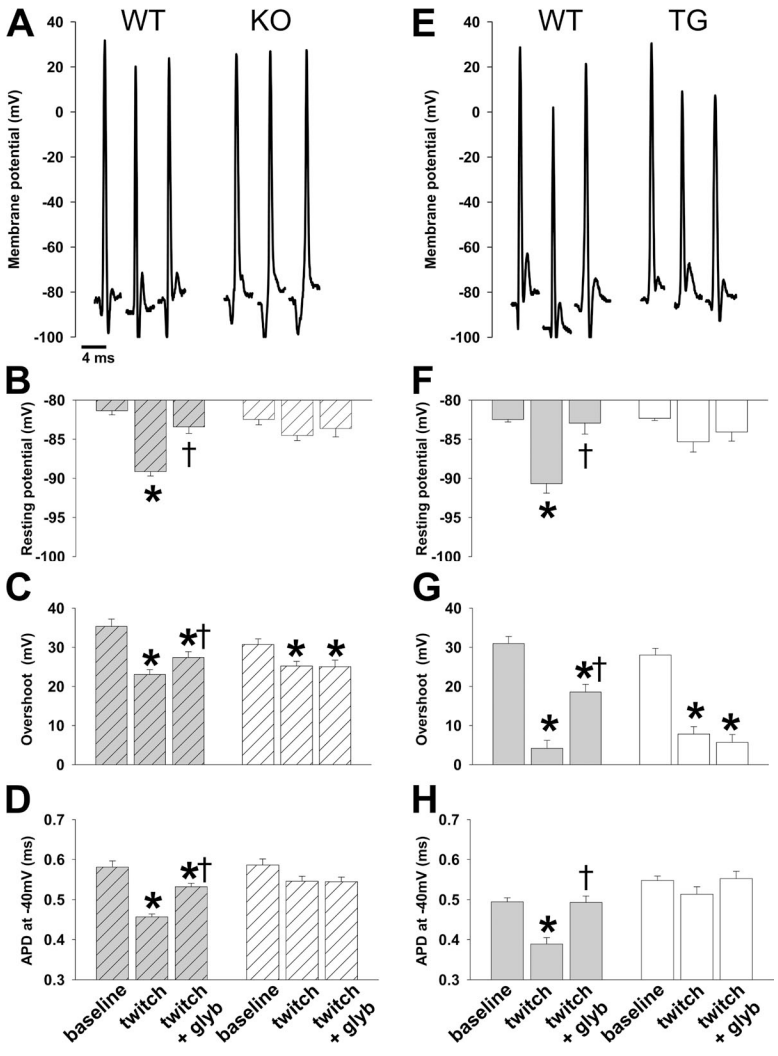

Figure 6. Low-frequency isometric muscle twitches result in K_{ATP} channel activation with significant changes in resting and action potentials. Representative action potentials and summary statistics for action potential morphology in TA muscle in situ are shown for KO and TG with their respective WT controls under the conditions indicated along the bottom of the figure (baseline, twitch, and twitch + glyb [glyburide]) according to the protocol illustrated in Fig. 5. Summary statistics for WT (gray with stripes) and KO (open with stripes) are shown on the left (n = 32, 80, and 44 APs from n = 5, 4, and 4 mice and 48, 113, and 33 APs from 6, 5, and 4 mice, respectively; *, $P < 0.05$ vs. baseline and †, $P < 0.05$ vs. twitch using Student's t test and Mann–Whitney rank sum test) and for WT (gray) and TG (open) on the right (n = 46, 20, and 30 APs from n = 9, 4, and 4 mice and 38, 26, and 32 APs from n = 11, 5, and 5 mice, respectively; *, $P < 0.05$ vs. baseline and †, $P < 0.05$ vs. twitch using Student's t test and Mann–Whitney rank sum test) under their respective representative action potentials. (A–D) Shown for WT controls with KO are representative action potentials (A), resting potential (−81.4 ± 0.5 mV, −89.2 ± 0.5 mV, and −83.4 ± 0.8 mV for WT and −82.5 ± 0.7 mV, −84.5 ± 0.6 mV, and −83.6 ± 1.1 mV for KO; B), action potential overshoot (35.3 ± 1.9 mV, 23.0 ± 1.3 mV, and 27.4 ± 1.5 mV for WT and 30.7 ± 1.5 mV, 25.2 ± 1.2 mV, and 25.0 ± 1.7 mV for KO; C), and APD_{-40mV} (0.58 ± 0.02 ms, 0.46 ± 0.01 ms, and 0.53 ± 0.01 ms for WT and 0.59 ± 0.02 ms, 0.55 ± 0.01 ms, and 0.55 ± 0.01 ms for KO; D). (E–H) Shown for WT controls with TG are representative action potentials (E), resting potential (−82.5 ± 0.3 mV, −90.7 ± 1.2 mV, and −82.9 ± 1.4 mV for WT and −82.3 ± 0.3 mV, −85.3 ± 1.3 mV, and −84.1 ± 1.2 mV for TG; F), action potential overshoot (31.0 ± 1.8 mV, 4.2 ± 2.0 mV, and 18.5 ± 2.0 mV for WT and 28.0 ± 1.7 mV, 7.8 ± 1.9 mV, and 5.7 ± 2.0 mV for TG; G), and APD_{-40mV} (0.49 ± 0.01 ms, 0.39 ± 0.02 ms, and 0.49 ± 0.02 ms for WT and 0.55 ± 0.01 ms, 0.51 ± 0.02 ms, and 0.55 ± 0.02 ms for KO; H). Error bars indicate SEM.

sarcolemmal K_{ATP} channels are also critical regulators of myocyte energy use under nonstressed, physiological states, including nonexercise activity–induced thermogenesis (Alekseev et al., 2010; Zingman et al., 2011). However, direct evidence that low-intensity workload activates skeletal muscle K_{ATP} channels with an effect on membrane electrical properties, myocyte function, and energetics has yet to be established.

In the present study, we find that low-frequency muscle twitching is sufficient to trigger opening of K_{ATP} channels, leading to membrane hyperpolarization, reduction in action potential overshoot, and shortened APD_{-40mV}. Intact skeletal muscle K_{ATP} channel function limits calcium release and muscle heat production, whereas disruption of skeletal muscle K_{ATP} channels results in excessive calcium release, muscle force development, and thermogenesis.

We used in situ recording of TA muscle to define changes in transmembrane resting and action potentials induced by low-frequency repetitive muscle twitching as a model of nonexercise activity. This approach, in which we maintain intact innervation, blood supply, interstitial relationships, and mechanical constraints, has an important advantage over traditional techniques in isolated muscle or myofiber preparations by assessing transmembrane resting and action potentials within a largely preserved physiological environment. A second advantage is the ability of this technique to directly and simultaneously probe membrane electrical properties and mechanical function (Brooks and Faulkner, 1988; Hakim et al., 2011). This approach is particularly relevant to the study of the physiological role of K_{ATP} channels, as their gating hinges on muscle cellular energetics which would be heavily influenced by experimental conditions.

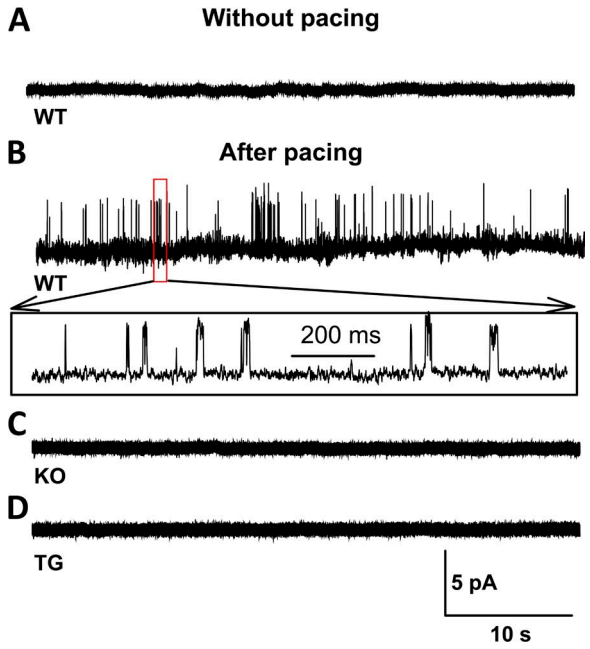

Figure 7. Low-frequency contractions induce K_{ATP} channel opening in isolated myofibers. (A–D) Representative examples of single channel recordings of K_{ATP} channel activity obtained by cell-attached patches in isolated FDB myofibers after resting (A) or within 20 s after cessation of 5 min of 1-Hz pacing in WT (B), KO (C), and TG (D). Each group consisted of five patches. K_{ATP} channel activity was provoked in all five WT patches, but none of the KO or TG patches.

K_{ATP} channel opening was previously linked to action potential amplitude reduction and prevention of excessive membrane depolarization (Cifelli et al., 2008; MacIntosh et al., 2012). Our in situ data differ from these electrophysiological studies performed on isolated muscles or myofibers in that they indicate that K_{ATP} channel opening in response to repetitive muscle twitching causes membrane hyperpolarization, rather than prevents excessive depolarization. The apparent differences can be related to several factors. First, in situ measurements could be expected to differ from those in an isolated preparation because of even small differences in muscle pH, temperature, energetics, and signaling. Second, we used lower muscle workloads and therefore significantly smaller changes in the intracellular environment can be expected. In skeletal myofibers, the presence of a large chloride conductance results in a resting potential above the potassium equilibrium (Hutter and Noble, 1960; Pedersen et al., 2005; Pierno et al., 2007; Lueck et al., 2010). Opening of skeletal muscle K_{ATP} channels would be expected to drive the membrane potential closer to the potassium equilibrium and thus explain the witnessed hyperpolarization. This is in contrast to findings in cardiomyocytes where the resting membrane potential is defined by a large potassium conductance, predominantly through IK_1 (Tomaselli and Marbán, 1999), such that opening of K_{ATP} channels does not appreciably affect the resting potential but only appears to affect the duration and amplitude of the action potential (Hodgson et al., 2003; Zingman et al., 2007; Flagg et al., 2010; Zhu et al., 2011).

As expected, K_{ATP} channel activation also reduces the skeletal muscle action potential overshoot and duration. The change in the overshoot is consistent with that of a previously published study (Gong et al., 2003). However, in contrast to the findings of others (Gong et al., 2003), we did detect a K_{ATP} channel–dependent decrease in APD. This discrepancy may be attributed to a difference in measurement technique as we compared APDs at −40 mV, the voltage above which calcium release is initiated (Delbono and Stefani, 1993; Szentesi et al., 1997). We chose this approach to better associate APD with calcium handling under conditions when both resting potential and amplitude are changed.

Our data also indicate that APD_{-40mV} may be a more important determinant of K_{ATP} channel–dependent effects on muscle function than action potential overshoot as under low-intensity workload, KO and TG skeletal muscle exhibited changes in calcium release, force, and

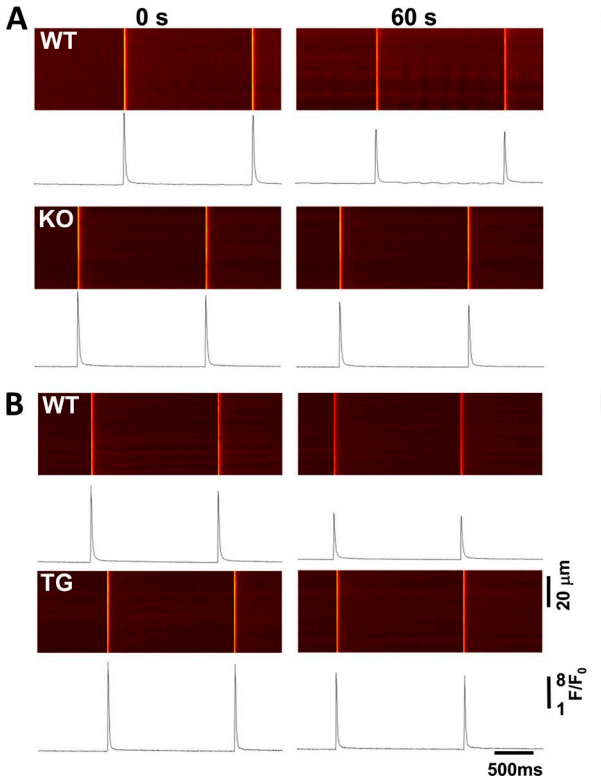

Figure 8. K_{ATP} channel deficiency results in greater calcium release in response to repetitive myofiber stimulation. (A and B) Representative confocal images and corresponding spatial average of Ca^{2+} fluorescence (F/F_0) in isolated FDB fibers are shown at 0 and 60 s of field stimulation at 1 Hz for C57BL/6 WT (top) and KO (bottom; A) and FVB WT (top) and TG (bottom; B). (C and D) The change in amplitude of the Ca^{2+} transients, normalized to the baseline levels at time 0, is shown for C57BL/6 WT ($n = 25$) and KO ($n = 18$) as a function of time (WT: percent baseline $F/F_0 = 0.89 \pm 0.01$, 0.82 ± 0.02, and 0.78 ± 0.02; and KO: percent baseline $F/F_0 = 0.91 \pm 0.01$, 0.86 ± 0.01, and 0.86 ± 0.02 at 20, 40, and 60 s, respectively; *, $P < 0.05$ for single pairwise comparisons between WT and KO values at each time point using Student's *t* test; C) and for FVB WT ($n = 8$) and TG ($n = 14$) as a function of time (WT: percent baseline $F/F_0 = 0.9 \pm 0.01$, 0.81 ± 0.02, and 0.76 ± 0.02; and TG: percent baseline $F/F_0 = 0.91 \pm 0.03$, 0.86 ± 0.03, and 0.83 ± 0.03 at 20, 40 and 60 s, respectively; *, $P < 0.05$ for single pairwise comparisons between WT and TG values at each time point using Student's *t* test; D). Error bars indicate SEM.

heat production in correlation with an observed lack of shortening of the APD_{-40mV}, but independent of changes in action potential overshoot, which were similar between KO or TG and their WT control muscles.

In spite of variable K_{ATP} channel expression in the IIB and IIX myofiber types in TA, we did not see segregation of the measured electrophysiological parameters. This is in line with our previous findings in cardiomyocytes, in which the level of K_{ATP} channel expression predominantly affected the rate of response rather than the magnitude (Zhu et al., 2011; Zingman et al., 2011). K_{ATP} channels open in response to a sensed reduction in cytosolic ATP and associated increase of ADP levels (Noma, 1983; Lederer and Nichols, 1989). However, as

TABLE 3

Calcium parameters for isolated myofibers

Calcium parameters	C57BL/6 WT		KO		FVB WT		TG	
Calcium transient parameters								
Time (s)	0	60	0	60	0	60	0	60
BG (AU)	22.6 ± 0.9	25.0 ± 1.2	20.5 ± 0.6 (P = NS)	21.7 ± 0.8 (P < 0.05)	20.0 ± 0.9	21.3 ± 1.0	18.9 ± 1.5 (P = NS)	18.7 ± 1.4 (P = NS)
F/F_0	7.5 ± 0.2	5.6 ± 0.3	8.3 ± 0.4 (P = NS)	7.2 ± 0.4 (P < 0.05)	7.7 ± 0.4	5.9 ± 0.4	8.4 ± 0.3 (P = NS)	6.9 ± 0.2 (P < 0.05)
Time to peak (ms)	8.2 ± 0.2	8.3 ± 0.1	8.3 ± 0.01 (P = NS)	8.6 ± 0.2 (P = NS)	8.8 ± 0.3	8.9 ± 0.3	8.9 ± 0.3 (P = NS)	8.8 ± 9.2 (P = NS)
T_{50} (ms)	11.1 ± 0.5	11.1 ± 0.6	11.4 ± 0.7 (P = NS)	12.3 ± 0.7 (P = NS)	9.4 ± 0.6	9.9 ± 0.9	8.5 ± 0.4 (P = NS)	8.5 ± 0.3 (P = NS)
Resting cytosolic calcium								
Time (s)	0	60	0	60	0	60	0	60
Intensity ratio 340 nm/380 nm	0.94 ± 0.04	0.99 ± 0.03	0.90 ± 0.01 (P = NS)	0.99 ± 0.01 (P = NS)	0.97 ± 0.02	1.05 ± 0.02	0.94 ± 0.03 (P = NS)	1.05 ± 0.02 (P = NS)

Summary statistics for calcium transient parameters of background intensity (BG), spatial average of Ca^{2+} fluorescence (F/F_0), time to peak, and 50% decay (T_{50}), as well as ratiometric quantification of resting cytosolic calcium concentration (intensity ratio 340 nm/380 nm) are displayed (p-values are for KO or TG vs. corresponding WT parameters using Student's *t* test). For calcium transient parameters, $n = 25$, 19, 8, and 14 for C57BL/6 WT, KO, FVB WT, and TG, respectively. For resting cytosolic calcium, $n = 6$, 17, 13, and 11 for C57BL/6 WT, KO, FVB WT, and TG, respectively.

bulk cytosolic ATP levels are well maintained even under stress conditions, it has been proposed that K_{ATP} channels respond to the changes of local ATP/ADP concentrations driven by ATPases within the diffusion-restricted submembrane space (Selivanov et al., 2004; Alekseev et al., 2012). Indeed, it has been established that cardiac K_{ATP} channels exist in large membrane macromolecular complexes with Na^+/K^+ ATPase and Na^+/Ca^{2+} exchangers and colocalize with Ca^{2+} channels and Ca^{2+}-ATPases (Korchev et al., 2000; Li et al., 2010). Thus, we speculate that in the compartmentalized cell, the level of K_{ATP} channel expression would affect the proximity of K_{ATP} channels to sites of energy consumption and thus the rate, but not the steady-state amplitude, of their membrane homeostatic response. It seems likely that that the different density of K_{ATP} channel expression observed in various skeletal muscle fiber types may similarly affect the rate of the membrane response, although these time courses were not examined here and rather will be the subject of future investigation. This phenomenon may be particularly important in skeletal myofibers given their unique anatomical and physiological characteristics, specifically their very long length, which would favor self-sufficient microdomains, and their local membrane action potential activation by distributed motor endplates.

The energy-controlling function of K_{ATP} channels is based on their ability to feed back changes in cellular energy availability into constraints on cellular energy utilization through alterations in membrane electrical events (Nichols and Lederer, 1991; Gong et al., 2000; Zingman et al., 2002, 2011; Thabet et al., 2005; Cifelli et al., 2007, 2008; Alekseev et al., 2010; MacIntosh et al., 2012). By sensing even minor changes in nucleotides (Abraham et al., 2002; Selivanov et al., 2004; Alekseev et al., 2010), K_{ATP} channels can decode cellular metabolic dynamics during regular daily activity. Indeed, we demonstrate here that K_{ATP} channel–driven changes in skeletal myocyte excitability in response to low-intensity workload ensured reduced calcium release, smaller temperature elevation, and a stable, or even marginally reduced, peak contraction force over the 7-min twitching protocol. The discrepancy between the observed large decrease in peak calcium observed in experiments using isolated myofibers and the milder dynamics of force development measured in the in situ experiments are consistent with activity-dependent potentiation in calcium sensitivity (MacIntosh. 2003). At the same time, muscles with disrupted K_{ATP} channel function demonstrated a significantly larger temperature rise and slight increases in peak contraction force over time. This is in line with previous studies that linked K_{ATP} channel opening to reduced oxygen consumption during physical activity (Alekseev et al., 2010) and reductions in contraction force (Renaud, 2002; Gong et al., 2003; Cifelli et al., 2008).

The assessment of muscle energy consumption based on measurement of muscle heat production in situ assumes that there are no differences in vascular regulation in response to muscle contractions between TG or KO and WT mice. Vascular perfusion was not tracked in this experiment, but our previous study of mice expressing the same transgene in cardiac tissue indicate no differences in the vascular regulation of these mice under basal and stress conditions and would not be expected since the transgene is not expressed in the vasculature (Zhu et al., 2011). The KO mice were created by global knockout of the Kir6.2 channel subunit, which is not expressed in vascular tissue, and thus no interference in vascular function is expected (Suzuki et al., 2001). Our previous study has revealed that cardiac function is similar under baseline conditions between KO and WT mice despite the expression of Kir6.2 in the myocardium (Zingman et al., 2002). Therefore, we interpret the observed changes in the temperature of the twitched muscle to be directly related to myocyte function. Future studies with direct evaluation of muscle blood supply may further clarify this point.

Muscle energy efficiency can be defined as the ratio of mechanical work output to the total metabolic cost,

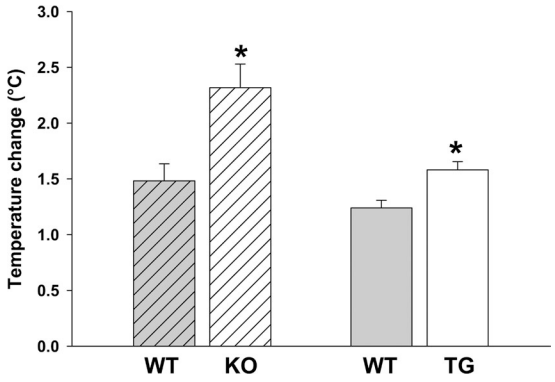

Figure 9. Skeletal muscles with genetic disruption of K_{ATP} channels generate greater heat with low-frequency repetitive twitching. In situ temperature, measured by thermocouples placed under the TA muscle, is displayed as the increase at 10 min of 1-Hz isometric twitching compared with baseline. The increase is 2.32 ± 0.21°C for KO (n = 3) and 1.48 ± 0.15°C for their WT controls (n = 8). The increase is 1.58 ± 0.08°C for TG (n = 3) and 1.24 ± 0.07°C for their WT controls (n = 3). *, $P < 0.05$ versus WT controls using Student's t test. Error bars indicate SEM.

which includes both force and heat liberation (Barclay et al., 2010). Here we exposed mice with normal and genetically disrupted K_{ATP} channel function to the equivalent low-intensity treadmill exercise to match their mechanical work output. Under this condition, we can interpret the larger rise of surface temperature in K_{ATP} channel–deficient mice as an indication of their energy inefficiency. These findings also identify skeletal muscle K_{ATP} channels as potentially attractive targets for interventions to modify energy efficiency.

Although an improvement over standard methods, our in situ floating microelectrode technique has some limitations. (a) We minimally alter the environment by our need to remove the muscle fascia and to superfuse the muscle to prevent drying. This may alter the normal accumulation of extracellular ions and thereby have some effect on resting potential and action potential morphology. (b) Because membrane electrical activity may be different between the surface of the muscle and the interior, our electrophysiological measurements might be somewhat dissociated from the corresponding mechanical measurements, which would be mostly defined by the greater mass of myofibers in the interior of the muscle bundle. (c) The applied drugs are presumed to penetrate to at least the depth of microelectrode impalement and therefore impact the measured transmembrane potentials, but are unlikely to penetrate into sufficient muscle mass to significantly affect the overall mechanical function of the muscle. However, taking these limitations into consideration, we believe this technique nonetheless is a valuable addition to the array of tools used to assess skeletal muscle electrophysiology.

In summary, this study demonstrates how sarcolemmal K_{ATP} channels function to control calcium handling and energy use in skeletal muscles even under mundane, low-intensity activity. Understanding the mechanisms and effects of K_{ATP} channel opening on muscle energy consumption may provide a foundation for novel strategies

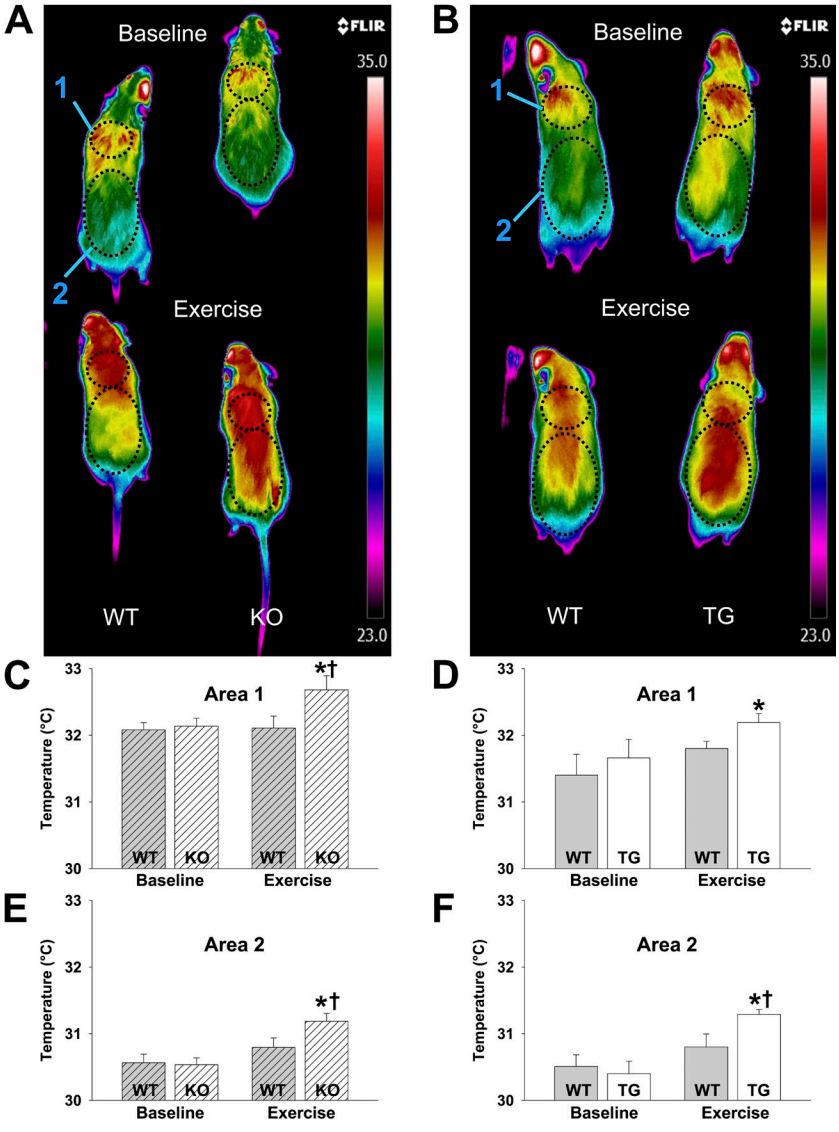

Figure 10. Absence of skeletal muscle K_{ATP} channels associated with excessive body heat production with low-intensity physical activity. (A and B) Representative thermal images at rest and with slow ambulation on a treadmill with the body surface areas of interest marked (area 1 = upper back at the shoulders, area 2 = lower back, including the hips) are shown for KO mice and their WT controls (A) and TG mice and their WT controls (B). (C and D) Summary statistics of temperature measured at rest and with exercise in area 1 are shown for KO (32.14 ± 0.12°C at rest [n = 20] and 32.68 ± 0.21°C with exercise [n = 15]) and their WT controls (32.08 ± 0.11°C at rest [n = 20] and 32.11 ± 0.18°C with exercise [n = 15]; C) and TG (31.66 ± 0.28°C at rest [n = 10] and 32.19 ± 0.14°C with exercise [n = 12]) and their WT controls (31.40 ± 0.31°C at rest [n = 10] and 31.80 ± 0.11°C with exercise [n = 12]; D). (E and F) Summary statistics of temperature measured at rest and with exercise in area 2 are shown for KO (30.54 ± 0.10°C at rest [n = 20] and 31.19 ± 0.12°C with exercise [n = 15]) and their WT controls (30.57 ± 0.13°C at rest [n = 20] and 30.79 ± 0.14°C with exercise [n = 15]; E) and TG (30.4 ± 0.19°C at rest [n = 11] and 31.29 ± 0.07°C with exercise [n = 12]) and their WT controls (30.51 ± 0.17°C at rest [n = 11] and 30.8 ± 0.20°C with exercise [n = 16]; F). *, $P < 0.05$ for TG and KO versus their respective WT controls using Student's t test. †, $P < 0.05$ for exercise versus rest temperature. Error bars indicate SEM.

for combating metabolic derangements, including muscle wasting and cachexia when energy conservation is required or obesity when energy dissipation is desired.

We are grateful to Dr. T. Miki (Chiba University, Chiba, Japan) and Dr. S. Seino (Kobe University, Kobe, Japan) for providing the Kir6.2-KO model, to Dr. A. Alekseev (Mayo Clinic, Rochester, MN) for thoughtful and valuable discussion, and to L. Yang (University of Iowa, Iowa City, IA) for maintenance of mouse colonies.

This work was supported by the National Institutes of Health (HL092286 and HL113089 to D.M. Hodgson-Zingman; HL093368 and DK092412 to L.V. Zingman; HL085820 to W.A. Coetzee; HL070250, HL096652, HL079031, and HL113001 to M.E. Anderson; AR052777 to D.J. Goldhamer; and HL090905 to L.-S. Song), the VA Merit Review Program (1I0BX000718 to L.V. Zingman), the Carver Trust (01-224 to D.M. Hodgson-Zingman), and the Fraternal Order of Eagles (to L.V. Zingman).

The authors have no conflicting financial interests.

Richard L. Moss served as editor.

Submitted: 15 July 2013
Accepted: 18 November 2013

REFERENCES

Abraham, M.R., V.A. Selivanov, D.M. Hodgson, D. Pucar, L.V. Zingman, B. Wieringa, P.P. Dzeja, A.E. Alekseev, and A. Terzic. 2002. Coupling of cell energetics with membrane metabolic sensing. Integrative signaling through creatine kinase phosphotransfer disrupted by M-CK gene knock-out. *J. Biol. Chem.* 277:24427–24434. http://dx.doi.org/10.1074/jbc.M201777200

Aguilar-Bryan, L., and J. Bryan. 1999. Molecular biology of adenosine triphosphate-sensitive potassium channels. *Endocr. Rev.* 20:101–135. http://dx.doi.org/10.1210/er.20.2.101

Alekseev, A.E., S. Reyes, S. Yamada, D.M. Hodgson-Zingman, S. Sattiraju, Z. Zhu, A. Sierra, M. Gerbin, W.A. Coetzee, D.J. Goldhamer, et al. 2010. Sarcolemmal ATP-sensitive K(+) channels control energy expenditure determining body weight. *Cell Metab.* 11:58–69. http://dx.doi.org/10.1016/j.cmet.2009.11.009

Alekseev, A.E., S. Reyes, V.A. Selivanov, P.P. Dzeja, and A. Terzic. 2012. Compartmentation of membrane processes and nucleotide dynamics in diffusion-restricted cardiac cell microenvironment. *J. Mol. Cell. Cardiol.* 52:401–409. http://dx.doi.org/10.1016/j.yjmcc.2011.06.007

Ashcroft, F.M. 1988. Adenosine 5′-triphosphate-sensitive potassium channels. *Annu. Rev. Neurosci.* 11:97–118. http://dx.doi.org/10.1146/annurev.ne.11.030188.000525

Ashcroft, F.M., and F.M. Gribble. 2000. New windows on the mechanism of action of K(ATP) channel openers. *Trends Pharmacol. Sci.* 21:439–445. http://dx.doi.org/10.1016/S0165-6147(00)01563-7

Banas, K., C. Clow, B.J. Jasmin, and J.M. Renaud. 2011. The KATP channel Kir6.2 subunit content is higher in glycolytic than oxidative skeletal muscle fibers. *Am. J. Physiol. Regul. Integr. Comp. Physiol.* 301:R916–R925. http://dx.doi.org/10.1152/ajpregu.00663.2010

Barclay, C.J., R.C. Woledge, and N.A. Curtin. 2010. Is the efficiency of mammalian (mouse) skeletal muscle temperature dependent? *J. Physiol.* 588:3819–3831. http://dx.doi.org/10.1113/jphysiol.2010.192799

Brooks, S.V., and J.A. Faulkner. 1988. Contractile properties of skeletal muscles from young, adult and aged mice. *J. Physiol.* 404:71–82.

Chen, J.C., J. Mortimer, J. Marley, and D.J. Goldhamer. 2005. MyoD-cre transgenic mice: a model for conditional mutagenesis and lineage tracing of skeletal muscle. *Genesis.* 41:116–121. http://dx.doi.org/10.1002/gene.20104

Cifelli, C., F. Bourassa, L. Gariépy, K. Banas, M. Benkhalti, and J.M. Renaud. 2007. KATP channel deficiency in mouse flexor digitorum brevis causes fibre damage and impairs Ca2+ release and force development during fatigue in vitro. *J. Physiol.* 582:843–857. http://dx.doi.org/10.1113/jphysiol.2007.130955

Cifelli, C., L. Boudreault, B. Gong, J.P. Bercier, and J.M. Renaud. 2008. Contractile dysfunctions in ATP-dependent K+ channel-deficient mouse muscle during fatigue involve excessive depolarization and Ca2+ influx through L-type Ca2+ channels. *Exp. Physiol.* 93:1126–1138. http://dx.doi.org/10.1113/expphysiol.2008.042572

Delbono, O., and E. Stefani. 1993. Calcium transients in single mammalian skeletal muscle fibres. *J. Physiol.* 463:689–707.

Flagg, T.P., D. Enkvetchakul, J.C. Koster, and C.G. Nichols. 2010. Muscle KATP channels: recent insights to energy sensing and myoprotection. *Physiol. Rev.* 90:799–829. http://dx.doi.org/10.1152/physrev.00027.2009

Gong, B., T. Miki, S. Seino, and J.M. Renaud. 2000. A K(ATP) channel deficiency affects resting tension, not contractile force, during fatigue in skeletal muscle. *Am. J. Physiol. Cell Physiol.* 279:C1351–C1358.

Gong, B., D. Legault, T. Miki, S. Seino, and J.M. Renaud. 2003. KATP channels depress force by reducing action potential amplitude in mouse EDL and soleus muscle. *Am. J. Physiol. Cell Physiol.* 285:C1464–C1474. http://dx.doi.org/10.1152/ajpcell.00278.2003

Gramolini, A., and J.M. Renaud. 1997. Blocking ATP-sensitive K+ channel during metabolic inhibition impairs muscle contractility. *Am. J. Physiol.* 272:C1936–C1946.

Hakim, C.H., D. Li, and D. Duan. 2011. Monitoring murine skeletal muscle function for muscle gene therapy. *Methods Mol. Biol.* 709:75–89. http://dx.doi.org/10.1007/978-1-61737-982-6_5

Hicks, A., and A.J. McComas. 1989. Increased sodium pump activity following repetitive stimulation of rat soleus muscles. *J. Physiol.* 414:337–349.

Hodgson, D.M., L.V. Zingman, G.C. Kane, C. Perez-Terzic, M. Bienengraeber, C. Ozcan, R.J. Gumina, D. Pucar, F. O'Coclain, D.L. Mann, et al. 2003. Cellular remodeling in heart failure disrupts K(ATP) channel-dependent stress tolerance. *EMBO J.* 22:1732–1742. http://dx.doi.org/10.1093/emboj/cdg192

Hutter, O.F., and D. Noble. 1960. The chloride conductance of frog skeletal muscle. *J. Physiol.* 151:89–102.

Inagaki, N., T. Gonoi, J.P. Clement IV, N. Namba, J. Inazawa, G. Gonzalez, L. Aguilar-Bryan, S. Seino, and J. Bryan. 1995. Reconstitution of IKATP: an inward rectifier subunit plus the sulfonylurea receptor. *Science.* 270:1166–1170. http://dx.doi.org/10.1126/science.270.5239.1166

Kefaloyianni, E., L. Bao, M.J. Rindler, M. Hong, T. Patel, E. Taskin, and W.A. Coetzee. 2012. Measuring and evaluating the role of ATP-sensitive K+ channels in cardiac muscle. *J. Mol. Cell. Cardiol.* 52:596–607. http://dx.doi.org/10.1016/j.yjmcc.2011.12.012

Korchev, Y.E., Y.A. Negulyaev, C.R. Edwards, I. Vodyanoy, and M.J. Lab. 2000. Functional localization of single active ion channels on the surface of a living cell. *Nat. Cell Biol.* 2:616–619. http://dx.doi.org/10.1038/35023563

Kristensen, M., and C. Juel. 2010. Potassium-transporting proteins in skeletal muscle: cellular location and fibre-type differences. *Acta Physiol. (Oxf.).* 198:105–123. http://dx.doi.org/10.1111/j.1748-1716.2009.02043.x

Lederer, W.J., and C.G. Nichols. 1989. Nucleotide modulation of the activity of rat heart ATP-sensitive K+ channels in isolated membrane patches. *J. Physiol.* 419:193–211.

Levine, J.A., L.M. Lanningham-Foster, S.K. McCrady, A.C. Krizan, L.R. Olson, P.H. Kane, M.D. Jensen, and M.M. Clark. 2005. Interindividual variation in posture allocation: possible role in human obesity. *Science.* 307:584–586. http://dx.doi.org/10.1126/science.1106561

Li, J., C.F. Kline, T.J. Hund, M.E. Anderson, and P.J. Mohler. 2010. Ankyrin-B regulates Kir6.2 membrane expression and function in

heart. *J. Biol. Chem.* 285:28723–28730. http://dx.doi.org/10.1074/jbc.M110.147868

Light, P.E., A.S. Comtois, and J.M. Renaud. 1994. The effect of glibenclamide on frog skeletal muscle: evidence for K+ATP channel activation during fatigue. *J. Physiol.* 475:495–507.

Lueck, J.D., A.E. Rossi, C.A. Thornton, K.P. Campbell, and R.T. Dirksen. 2010. Sarcolemmal-restricted localization of functional ClC-1 channels in mouse skeletal muscle. *J. Gen. Physiol.* 136:597–613. http://dx.doi.org/10.1085/jgp.201010526

MacIntosh, B.R. 2003. Role of calcium sensitivity modulation in skeletal muscle performance. *News Physiol. Sci.* 18:222–225.

MacIntosh, B.R., R.J. Holash, and J.M. Renaud. 2012. Skeletal muscle fatigue—regulation of excitation-contraction coupling to avoid metabolic catastrophe. *J. Cell Sci.* 125:2105–2114. http://dx.doi.org/10.1242/jcs.093674

Malester, B., X. Tong, I. Ghiu, A. Kontogeorgis, D.E. Gutstein, J. Xu, K.D. Hendricks-Munoz, and W.A. Coetzee. 2007. Transgenic expression of a dominant negative K(ATP) channel subunit in the mouse endothelium: effects on coronary flow and endothelin-1 secretion. *FASEB J.* 21:2162–2172. http://dx.doi.org/10.1096/fj.06-7821com

Matar, W., T.M. Nosek, D. Wong, and J. Renaud. 2000. Pinacidil suppresses contractility and preserves energy but glibenclamide has no effect during muscle fatigue. *Am. J. Physiol. Cell Physiol.* 278:C404–C416.

Matar, W., J.A. Lunde, B.J. Jasmin, and J.M. Renaud. 2001. Denervation enhances the physiological effects of the K(ATP) channel during fatigue in EDL and soleus muscle. *Am. J. Physiol. Regul. Integr. Comp. Physiol.* 281:R56–R65.

Miki, T., K. Nagashima, F. Tashiro, K. Kotake, H. Yoshitomi, A. Tamamoto, T. Gonoi, T. Iwanaga, J. Miyazaki, and S. Seino. 1998. Defective insulin secretion and enhanced insulin action in KATP channel-deficient mice. *Proc. Natl. Acad. Sci. USA.* 95:10402–10406. http://dx.doi.org/10.1073/pnas.95.18.10402

Minami, K., T. Miki, T. Kadowaki, and S. Seino. 2004. Roles of ATP-sensitive K+ channels as metabolic sensors: studies of Kir6.x null mice. *Diabetes.* 53:S176–S180. http://dx.doi.org/10.2337/diabetes.53.suppl_3.S176

Moreau, C., H. Jacquet, A.L. Prost, N. D'hahan, and M. Vivaudou. 2000. The molecular basis of the specificity of action of K(ATP) channel openers. *EMBO J.* 19:6644–6651. http://dx.doi.org/10.1093/emboj/19.24.6644

Nichols, C.G., and W.J. Lederer. 1991. Adenosine triphosphate-sensitive potassium channels in the cardiovascular system. *Am. J. Physiol.* 261:H1675–H1686.

Nichols, C.G., G.K. Singh, and D.K. Grange. 2013. KATP channels and cardiovascular disease: suddenly a syndrome. *Circ. Res.* 112:1059–1072. http://dx.doi.org/10.1161/CIRCRESAHA.112.300514

Noma, A. 1983. ATP-regulated K+ channels in cardiac muscle. *Nature.* 305:147–148. http://dx.doi.org/10.1038/305147a0

Pedersen, T.H., F. de Paoli, and O.B. Nielsen. 2005. Increased excitability of acidified skeletal muscle: role of chloride conductance. *J. Gen. Physiol.* 125:237–246. http://dx.doi.org/10.1085/jgp.200409173

Pierno, S., J.F. Desaphy, A. Liantonio, A. De Luca, A. Zarrilli, L. Mastrofrancesco, G. Procino, G. Valenti, and D. Conte Camerino. 2007. Disuse of rat muscle in vivo reduces protein kinase C activity controlling the sarcolemma chloride conductance. *J. Physiol.* 584:983–995. http://dx.doi.org/10.1113/jphysiol.2007.141358

Renaud, J.M. 2002. Modulation of force development by Na+, K+, Na+ K+ pump and KATP channel during muscular activity. *Can. J. Appl. Physiol.* 27:296–315. http://dx.doi.org/10.1139/h02-017

Schwappach, B., N. Zerangue, Y.N. Jan, and L.Y. Jan. 2000. Molecular basis for K(ATP) assembly: transmembrane interactions mediate association of a K+ channel with an ABC transporter. *Neuron.* 26:155–167. http://dx.doi.org/10.1016/S0896-6273(00)81146-0

Seino, S., and T. Miki. 2003. Physiological and pathophysiological roles of ATP-sensitive K+ channels. *Prog. Biophys. Mol. Biol.* 81:133–176. http://dx.doi.org/10.1016/S0079-6107(02)00053-6

Selivanov, V.A., A.E. Alekseev, D.M. Hodgson, P.P. Dzeja, and A. Terzic. 2004. Nucleotide-gated KATP channels integrated with creatine and adenylate kinases: amplification, tuning and sensing of energetic signals in the compartmentalized cellular environment. *Mol. Cell. Biochem.* 256–257:243–256. http://dx.doi.org/10.1023/B:MCBI.0000009872.35940.7d

Shyng, S., T. Ferrigni, and C.G. Nichols. 1997. Regulation of KATP channel activity by diazoxide and MgADP. Distinct functions of the two nucleotide binding folds of the sulfonylurea receptor. *J. Gen. Physiol.* 110:643–654. http://dx.doi.org/10.1085/jgp.110.6.643

Sierra, A., Z. Zhu, N. Sapay, V. Sharotri, C.F. Kline, E.D. Luczak, E. Subbotina, A. Sivaprasadarao, P.M. Snyder, P.J. Mohler, et al. 2013. Regulation of cardiac ATP-sensitive potassium channel surface expression by calcium/calmodulin-dependent protein kinase II. *J. Biol. Chem.* 288:1568–1581. http://dx.doi.org/10.1074/jbc.M112.429548

Skirboll, L.R., R.A. Howard, and K.L. Dretchen. 1979. The effect of verapamil on the gastrocnemius and soleus muscles of the cat in vivo. *Eur. J. Pharmacol.* 60:15–21. http://dx.doi.org/10.1016/0014-2999(79)90047-5

Song, L.S., E.A. Sobie, S. McCulle, W.J. Lederer, C.W. Balke, and H. Cheng. 2006. Orphaned ryanodine receptors in the failing heart. *Proc. Natl. Acad. Sci. USA.* 103:4305–4310. http://dx.doi.org/10.1073/pnas.0509324103

Suzuki, M., R.A. Li, T. Miki, H. Uemura, N. Sakamoto, Y. Ohmoto-Sekine, M. Tamagawa, T. Ogura, S. Seino, E. Marbán, and H. Nakaya. 2001. Functional roles of cardiac and vascular ATP-sensitive potassium channels clarified by Kir6.2-knockout mice. *Circ. Res.* 88:570–577. http://dx.doi.org/10.1161/01.RES.88.6.570

Suzuki, M., N. Sasaki, T. Miki, N. Sakamoto, Y. Ohmoto-Sekine, M. Tamagawa, S. Seino, E. Marbán, and H. Nakaya. 2002. Role of sarcolemmal K(ATP) channels in cardioprotection against ischemia/reperfusion injury in mice. *J. Clin. Invest.* 109:509–516.

Szentesi, P., V. Jacquemond, L. Kovács, and L. Csernoch. 1997. Intramembrane charge movement and sarcoplasmic calcium release in enzymatically isolated mammalian skeletal muscle fibres. *J. Physiol.* 505:371–384. http://dx.doi.org/10.1111/j.1469-7793.1997.371bb.x

Thabet, M., T. Miki, S. Seino, and J.M. Renaud. 2005. Treadmill running causes significant fiber damage in skeletal muscle of KATP channel-deficient mice. *Physiol. Genomics.* 22:204–212. http://dx.doi.org/10.1152/physiolgenomics.00064.2005

Tomaselli, G.F., and E. Marbán. 1999. Electrophysiological remodeling in hypertrophy and heart failure. *Cardiovasc. Res.* 42:270–283. http://dx.doi.org/10.1016/S0008-6363(99)00017-6

Tong, X., L.M. Porter, G. Liu, P. Dhar-Chowdhury, S. Srivastava, D.J. Pountney, H. Yoshida, M. Artman, G.I. Fishman, C. Yu, et al. 2006. Consequences of cardiac myocyte-specific ablation of KATP channels in transgenic mice expressing dominant negative Kir6 subunits. *Am. J. Physiol. Heart Circ. Physiol.* 291:H543–H551. http://dx.doi.org/10.1152/ajpheart.00051.2006

Vivaudou, M., and C. Forestier. 1995. Modification by protons of frog skeletal muscle KATP channels: effects on ion conduction and nucleotide inhibition. *J. Physiol.* 486:629–645.

Weiss, J.N., and N. Venkatesh. 1993. Metabolic regulation of cardiac ATP-sensitive K+ channels. *Cardiovasc. Drugs Ther.* 7:499–505. http://dx.doi.org/10.1007/BF00877614

Zhang, M.Y., W.J. Zhang, and S. Medler. 2010. The continuum of hybrid IIX/IIB fibers in normal mouse muscles: MHC isoform proportions and spatial distribution within single fibers. *Am. J. Physiol. Regul. Integr. Comp. Physiol.* 299:R1582–R1591. http://dx.doi.org/10.1152/ajpregu.00402.2010

Zhou, X., P. Guse, P.D. Wolf, D.L. Rollins, W.M. Smith, and R.E. Ideker. 1992. Existence of both fast and slow channel activity during

the early stages of ventricular fibrillation. *Circ. Res.* 70:773–786. http://dx.doi.org/10.1161/01.RES.70.4.773

Zhu, Z., C.M. Burnett, G. Maksymov, E. Stepniak, A. Sierra, E. Subbotina, M.E. Anderson, W.A. Coetzee, D.M. Hodgson-Zingman, and L.V. Zingman. 2011. Reduction in number of sarcolemmal KATP channels slows cardiac action potential duration shortening under hypoxia. *Biochem. Biophys. Res. Commun.* 415:637–641. http://dx.doi.org/10.1016/j.bbrc.2011.10.125

Zingman, L.V., A.E. Alekseev, M. Bienengraeber, D. Hodgson, A.B. Karger, P.P. Dzeja, and A. Terzic. 2001. Signaling in channel/enzyme multimers: ATPase transitions in SUR module gate ATP-sensitive K+ conductance. *Neuron.* 31:233–245. http://dx.doi.org/10.1016/S0896-6273(01)00356-7

Zingman, L.V., D.M. Hodgson, P.H. Bast, G.C. Kane, C. Perez-Terzic, R.J. Gumina, D. Pucar, M. Bienengraeber, P.P. Dzeja, T. Miki, et al. 2002. Kir6.2 is required for adaptation to stress. *Proc. Natl. Acad. Sci. USA.* 99:13278–13283. http://dx.doi.org/10.1073/pnas.212315199

Zingman, L.V., D.M. Hodgson, A.E. Alekseev, and A. Terzic. 2003. Stress without distress: homeostatic role for K(ATP) channels. *Mol. Psychiatry.* 8:253–254. http://dx.doi.org/10.1038/sj.mp.4001323

Zingman, L.V., A.E. Alekseev, D.M. Hodgson-Zingman, and A. Terzic. 2007. ATP-sensitive potassium channels: metabolic sensing and cardioprotection. *J. Appl. Physiol.* 103:1888–1893. http://dx.doi.org/10.1152/japplphysiol.00747.2007

Zingman, L.V., Z. Zhu, A. Sierra, E. Stepniak, C.M. Burnett, G. Maksymov, M.E. Anderson, W.A. Coetzee, and D.M. Hodgson-Zingman. 2011. Exercise-induced expression of cardiac ATP-sensitive potassium channels promotes action potential shortening and energy conservation. *J. Mol. Cell. Cardiol.* 51:72–81. http://dx.doi.org/10.1016/j.yjmcc.2011.03.010